Thermochimica Acta 511 (2010) 140–146

Contents lists available at ScienceDirect

Thermochimica Acta

journal homepage: www.elsevier.com/locate/tca

Effect of PVC on ionic conductivity, crystallographic structural, morphological and thermal characterizations in PMMA–PVC blend-based polymer electrolytes

S. Ramesh[a,*], Chiam-Wen Liew[b], Ezra Morris[b], R. Durairaj[b]

[a] Centre for Ionics University Malaya, Department of Physics, Faculty of Science, University of Malaya, Lembah Pantai, 50603 Kuala Lumpur, Malaysia
[b] Faculty of Engineering & Science, Universiti Tunku Abdul Rahman, Setapak, 53300 Kuala Lumpur, Malaysia

ARTICLE INFO

Article history:
Received 15 December 2009
Received in revised form 18 July 2010
Accepted 6 August 2010
Available online 13 August 2010

Keywords:
Polymer blend
Temperature dependence ionic conductivity
XRD
SEM
DSC
TGA

ABSTRACT

In this paper, temperature dependence of ionic conductivity, crystallographic structural, morphological and thermal characteristics of polymer blends of PMMA and PVC with lithium bis(trifluoromethanesulfonyl) imide (LiTFSI) as a dopant salt are investigated. The study on the temperature dependence of ionic conductivity shows that these polymer blends exhibit Arrhenius behavior. The highest ionic conductivity was achieved when 70 wt% of PMMA was blended with 30 wt% of PVC. X-ray diffraction (XRD) and scanning electron microscopy (SEM) reveal the amorphous nature and surface morphology of polymer electrolytes, respectively. In DSC analysis it was found that the glass transition temperature (T_g) and melting temperature (T_m) decreased, whereas the decomposition temperature (T_d) increased. In contrast, the shift towards higher decomposition temperature and decrease in weight loss of polymer electrolytes, in TGA studies, indicates that the thermal stability of polymer electrolytes improved.

1. Introduction

Recent developments in solid state ionic conductors, such as insertion compounds, fast/superionic conductors, polymer electrolytes, and the development of new solid state materials for electrodes have drawn keen interest from the researchers working in the area of electrical power generation and storage systems. Among these, the recent ones are the polymer electrolytes also known as polyelectrolytes [1]. Solid polymer electrolytes (SPEs) are promising materials because of its wider applications in electrochromic windows (ECWs), modified electrodes, sensors, supercapacitors, electric vehicles (EV), high vacuum electrochemistry, thermoelectric generators and fuel cells [1,2]. However, much attention had been focused on the secondary lithium batteries.

SPEs are expected to replace conventional liquid electrolytes because they tend to eliminate the problems of corrosive solvent leakage and harmful gas production. They exhibit a wider electrochemical and thermal stability as well as low volatility [3–7]. The other advantages of SPEs are viz., they are light in weight, easy to process due to its flexibility, high energy density, high ionic conductivity and high automation process [8,9]. Many investigations on polymer blending [10,11], comb-branched copolymers [12,13], cross-linking polymer matrices [14,15], incorporation of additives like plasticizers [16,9], reinforcement by inorganic fillers [17,18], binary salt systems [19] and different preparation methods [20] were done in order to achieve higher ionic conductivity at ambient temperature. Among all the above-mentioned techniques, polymer blending is the most feasible technique. This technique complements the advantages from other techniques but also improves the electrical and physical properties of polymer electrolytes [21].

The amorphous nature of polymer matrix is associated with the high ionic conductivity of SPEs at ambient temperature. Several methods including X-ray diffraction (XRD) and differential scanning calorimetry (DSC) were used to examine the crystal structures and crystalline nature of the polymer matrix. Scanning electron microscopy (SEM) is widely used to characterize the structural, morphological and crystallite size of SPEs. DSC measurement provides a quantitative study of thermal transitions of matrix polymer in polymer electrolytes by heating the polymer sample and an inert reference. Thermogravimetric analysis (TGA) is another versatile thermal analysis to investigate the thermal properties of SPEs as a function of change in temperature by determining the thermal stability of polymer electrolytes. The temperature dependence of ionic conductivity is extensively used in the study of ionic conduction mechanism of SPEs.

In the present work, the weight ratio of LiTFSI remains fixed in all the samples and the PMMA is blended with PVC at different weight

* Corresponding author. Tel.: +60 3 7967 4391.
E-mail address: rameshtsubra@gmail.com (S. Ramesh).

0040-6031/$ – see front matter © 2010 Elsevier B.V. All rights reserved.
doi:10.1016/j.tca.2010.08.005

ratios, so that we can find the optimum ratio of PMMA and PVC that exhibits the highest ionic conductivity. The structural studies (XRD and SEM) and thermal studies (DSC and TGA) of these polymer complexes with different weight ratios of PMMA and PVC were then conducted and is reported.

2. Experimental

2.1. Materials

In this study, PMMA with an average molecular weight of 350,000 g mol^{-1} (Aldrich), high molecular weight of PVC (Fluka), inorganic dopant salt LiTFSI (Fluka) and solvent THF (J.T. Baker) were used without further purification. Solution casting technique was used to prepare the thin films of polymer electrolytes used in this study.

2.2. Preparation of thin films

Prior to the preparation of the polymer electrolytes, LiTFSI was dried at 100 °C for 1 h to eliminate trace amounts of water in the material. The compositions prepared were [xPMMA–(1 − x)PVC], where x is 0.1, 0.5 and 0.7 and the weight ratio of polymer blend to lithium salt is 90:10. Table 1 shows the compositions and designations of particular polymer electrolytes. Appropriate amounts of PMMA, PVC and LiTFSI were dissolved in THF. The solution was stirred continuously for 24 h to obtain a homogenous mixture at room temperature. The solution was cast on a glass Petri dish and was allowed to evaporate slowly inside a fume hood. This process will produce a mechanically stable and a free standing thin film.

2.3. Characterizations

2.3.1. Temperature dependence analysis

The prepared samples were subjected to AC-impedance spectroscopy for ionic conductivity studies. The thicknesses of the thin films were measured by using a micrometer screw gauge. The ionic conductivities of the samples were determined, by using HIOKI 3532-50 LCR HiTESTER, over the frequency range of 50 Hz to 1 MHz and from ambient temperature until 80 °C. Two stainless steel (SS) blocking electrodes were used in this study with the con SS/SPE/SS.

2.3.2. X-ray diffraction (XRD)

The amorphousity of polymer electrolytes was investigated using XRD. The XRD patterns were recorded on a Siemens D 5000 diffractometer with Cu-Kα radiation (λ = 1.54060 Å), over the range of 2θ = 5–80° at ambient temperature.

2.3.3. Scanning electron microscopy (SEM)

Using Leica's SEM (model S440) at 10 kV, the morphology of polymer blends at room temperature was studied. Insulators such as pure PMMA, PVC and PMMA–PVC samples were coated with a thin layer of gold to prevent electrostatic charging.

2.3.4. Differential scanning calorimetry (DSC)

DSC analysis was carried out, under nitrogen flow rate of 50 ml min^{-1}, using a METTLER TOLEDO Thermal Analyzer which comprised of DSC 823^e as the main unit and STARe software. Samples weighing approximately 2–3 mg were hermetically sealed in a 40 μl aluminum crucible. The samples were heated from 25 to 105 °C to remove any traces of solvent and water. The temperature was then maintained at 105 °C for 2 min to ensure the complete evaporation. The samples were then cooled rapidly to 25 °C and then reheated to 450 °C at a heating rate of 10 °C min^{-1}. The final heating scan was used to evaluate the T_g, T_m and T_d. The mid point of endothermic reaction is assigned as T_g. The endothermic peak point of melting and decomposition are assigned as T_m and T_d, respectively.

2.3.5. Thermogravimetric analysis (TGA)

TGA was carried out using a METTLER TOLEDO Thermal Gravimetric Analyser which comprised of TGA/SDTA851^e as the main unit and STARe software. Samples weighing 2–3 mg were placed in a 150 μl silica crucible. The samples were then heated from 30 to 400 °C at a heating rate of 10 °C min^{-1} under nitrogen flow rate of 10 ml min^{-1}.

3. Result and discussion

3.1. Temperature dependence ionic conductivity studies

Fig. 1 depicts the Arrhenius plot of PE 3, PE 5 and PE 9 which shows that the ionic conductivity increases with temperature. This is attributed to the expansion of polymer matrix. The polymer matrix expands with increase in temperature, which results in the formation of free volume and empty spaces for the migration of ions. This assists the mobility of ions and minimizes the effect of ion clouds at the electrode and electrolyte interface [22,23]. The vibrational mode of polymer segments also increases with the increase in temperature. As a result, the polymer segments have sufficient energy to overcome the hydrostatic pressure which is imposed by its surrounding atoms. This results in the formation of voids and facilitates the segmental transportation of charge carriers. Hence there is an increase in ionic conductivity [9].

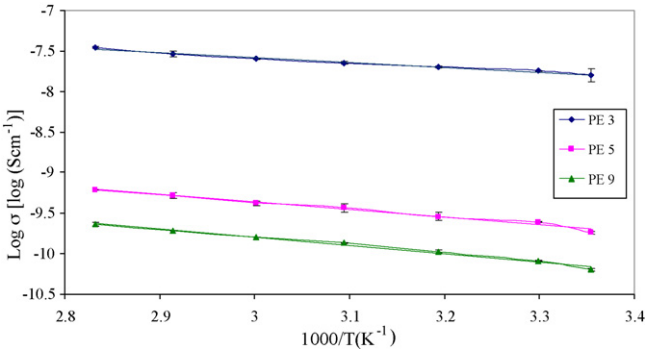

Fig. 1. Arrhenius plot of ionic conductivity of PE 3, PE 5 and PE 9.

Table 1
Compositions, designations, activation energy and DSC measurements of PMMA–PVC–LiTFSI based polymer electrolytes.

Composition of PMMA and PVC (wt%)		Designations	Activation energy, E_a (eV)	DSC measurements		
PMMA	PVC			T_g	T_m	T_d
70	30	PE 3	0.12021	115.12	185.12	345.38, 388.01
50	50	PE 5	0.18724	65.40, 125.09	192.13	335.16, 387.05
10	90	PE 9	0.20393	66.23, 134.98	235.06	315.21, 386.31

As shown in Fig. 1, the regression values are close to unity, indicating the presence of Arrhenius behavior. In this rule, the conductivity is expressed as:

$$\sigma = A \exp\left(\frac{-E_a}{kT}\right)$$

where A is a constant which is proportional to the amount of charge carriers, E_a is activation energy, k is Boltzmann constant and T represents the absolute temperature in K. In general, this theory follows the hopping mechanism which states that the interaction of polar group of the polymeric chain with Li^+ is weaker and hence these charge carriers are decoupled from the segmental motion of polymer matrix. This creates vacant sites in the polymer chain. Therefore, the ions from adjacent sites tend to occupy these neighboring vacant sites and form the coordination with the polymer chain. Fig. 1 shows that ionic conductivity of PE 3 is greater than PE 5 and that of PE 5 is greater than PE 9. The amorphous nature of PE 3 increases as the content of PMMA increases in comparison with PE 5 and PE 9. The increase in amorphous region leads to the disorder mode of segmental polymer chain and thus forms more free voids for ionic conduction. This promotes the ion transportation and hence the increase in ionic conductivity [24].

The lower ionic conductivity of the polymer electrolyte is attributed to excessive cross-linking effect. Higher amount of PVC incorporated in the polymer electrolytes leads to high degree of cross-linking between PMMA and PVC and increases the viscosity by forming entanglements within the polymer chain. As a result, free space for ion transportation is reduced and then impedes the mobility of charge carriers. Consequently, the ionic conductivity is decreased [18]. The mechanism of cross-linking is further discussed in Section 3.4.

The activation energy, E_a, is also determined in this study. As discussed earlier, the Li^+ tends to dissociate from the polymer chain and other Li^+ ions from the surrounding favor to coordinate with the polymer chain with the aid of segmental motion of polymer chain. Energy is required to overcome this reorganization and reformation of the polymer chain with Li^+. This energy is defined as activation energy. As shown in Table 1, E_a is inversely proportional to ionic conductivity. This is mainly attributed to the amorphous region in the polymer matrix. The degree of amorphous phase leads to the disorderly arrangement of molecules in the polymer matrix which results in a more flexible polymer chain. Therefore, the attractive bonds between the macromolecules become weaker and requiring less energy to break the bond for reorganization and reformation of coordination with Li^+. This enhances the Li^+ diffusivity in the polymer matrix [18]. Based on the above discussion it can be concluded that the hopping process is favorable with decreasing E_a.

3.2. X-ray diffraction (XRD) studies

Figs. 2 and 3 illustrate the XRD diffractograms of pure PMMA, pure PVC, PMMA–PVC, pure LiTFSI and PMMA–PVC blend-based polymer electrolytes. From Fig. 2(a), a broad characteristic peak of PMMA was obtained at angles of $2\theta = 16.4^\circ$ with a shoulder at $2\theta = 22.5^\circ$ which reveals the amorphous phase of PMMA. The intensity of these characteristic peaks is decreased after the impregnation of PVC. This implies that the addition of PVC disrupted the arrangement in the polymer backbone of PMMA [25]. The presence of interactions between PMMA and PVC, such as cross-linking, is attributed to this phenomenon. Complexation of PMMA and PVC occurs with the aid of these interactions and it is further discussed in Section 3.4. Apart from the peak intensity of these characteristic peaks, another evidence of complexation is observed. The blending of PMMA with PVC shifts the peaks at $2\theta = 16.4^\circ$ and $2\theta = 22.5^\circ$ to 15.8° and 22.3°, revealing the change in crystallographic organization [19].

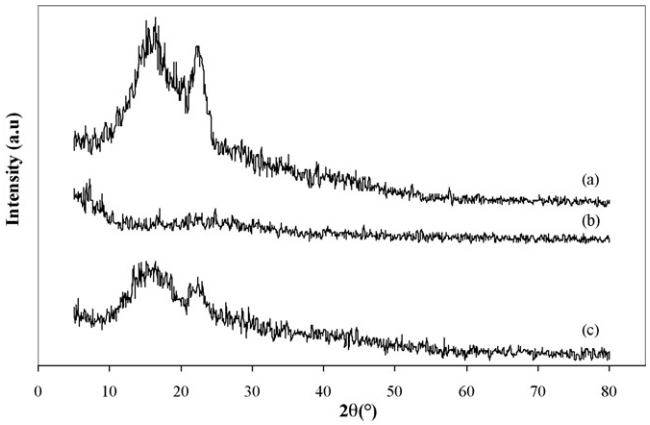

Fig. 2. XRD patterns of (a) pure PMMA, (b) pure PVC and (c) PMMA–PVC.

Fig. 3(a) illustrates the sharp intense peaks at $2\theta = 13.6^\circ$, 15.9°, 18.6°, 18.9° and 21.4° and reveals the crystalline character of LiTFSI. These crystalline peaks were disappeared in PMMA–PVC blend-based polymer electrolytes. The absence of excess salt indicates that LiTFSI is fully complexed with PMMA and PVC [9]. A complete dissolution in the polymer electrolytes leads to a complexation between PMMA, PVC and LiTFSI [26]. Absence of these crystalline peaks in polymer blended electrolytes indicates that the electrolytes are in amorphous region. As shown in Fig. 3, the characteristic peaks of PMMA–PVC at $2\theta = 15.8^\circ$ and $2\theta = 22.3^\circ$ are shifted to 2θ angles of 16.9° and 22.6° for PE 3, to 16.1° and 22.4° for PE 5 and to 16.4° and 22.7° for PE 9. This variation confirms the complexation between PMMA–PVC polymer blends and LiTFSI [25]. The presence of complexation has been further confirmed based on the changes in peak intensity. It can be seen by comparing Fig. 2(c) with Fig. 3(b)–(d) that the characteristic peak intensity decreases upon incorporation of LiTFSI. It can be inferred from the above comparison that the degree of crystallinity decreases and hence increases the amorphous region in polymer electrolytes which leads to higher ionic conductivity [27]. As discussed in Section 3.1, the amorphous behavior increases with PMMA concentration. It has been proved in this study that the intensity of characteristic peak reduces upon the addition of higher PMMA loadings. Comparing the intensity of characteristic peaks of PE 3, PE 5 and PE 9, PE 3 has the lowest which implies that PE 3 has more amorphous behavior. This increment in amorphous character improves the ionic transportation in the polymer matrix and induces the highest ionic conductivity. In other words, higher loading of PVC in polymer electrolytes impedes

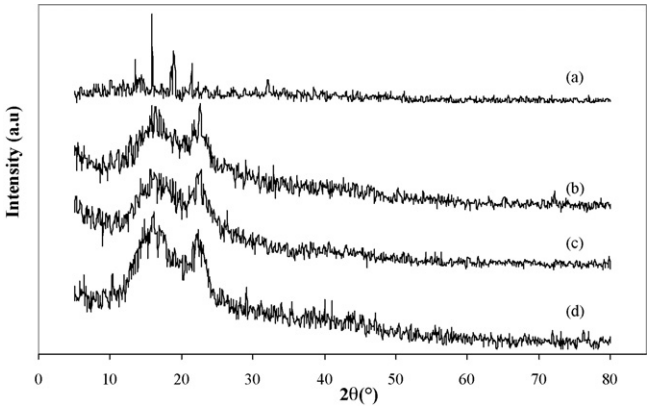

Fig. 3. XRD patterns of (a) Pure LiTFSI, (b) PE 3, (c) PE 5 and (d) PE 9.

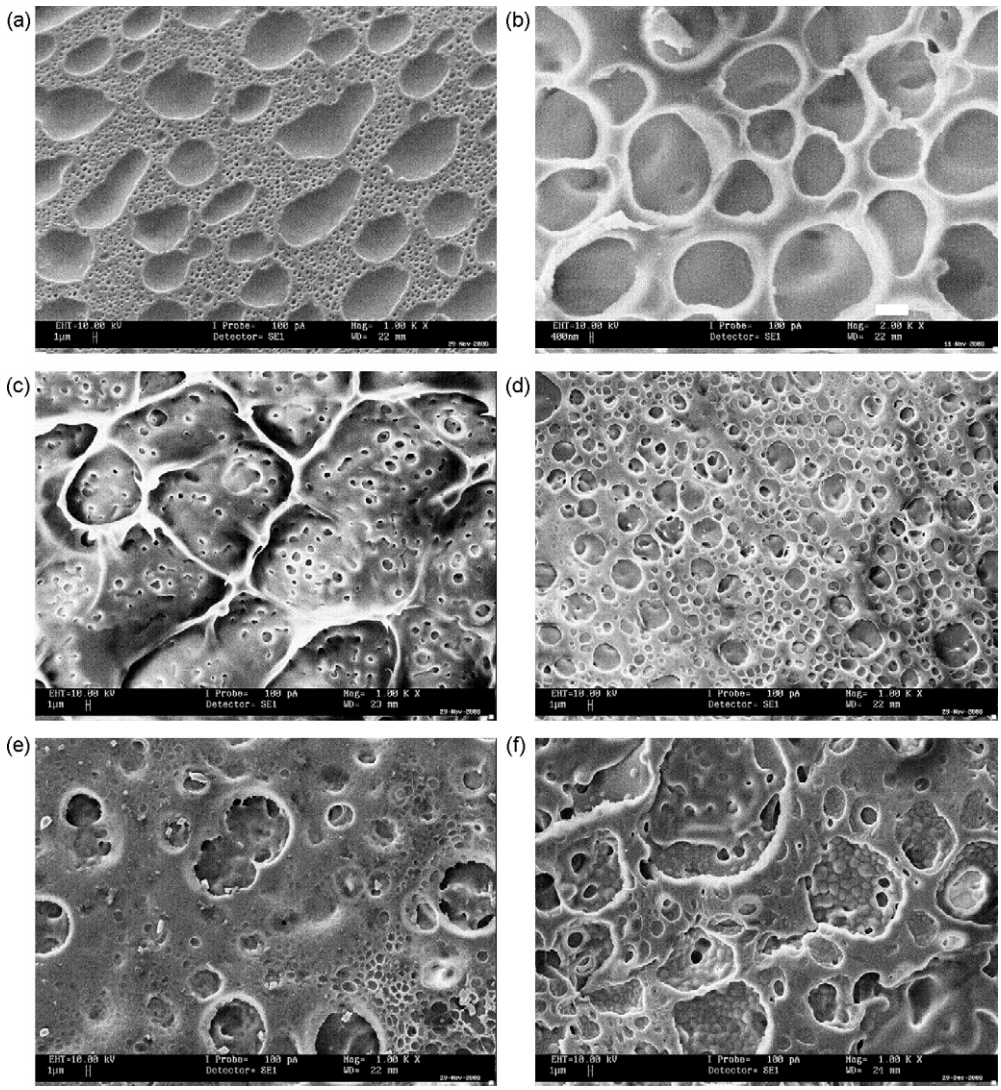

Fig. 4. SEM image of (a) pure PMMA, (b) pure PVC, (c) PMMA–PVC, (d) PE 3, (e) PE 5 and (f) PE 9.

the ion mobility by forming entanglements in the polymer network via cross-linking, thus leading to lower ionic conductivity.

3.3. Scanning electron microscopy (SEM) studies

SEM images of PMMA, PVC and polymer blend electrolytes are shown in Fig. 4(a)–(f). Small craters with average pore size of 1 and 2 μm have formed on the pure PMMA and PMMA–PVC respectively and this is ascribed to the evaporation of THF solvent during the preparation of thin film [28]. From Fig. 4(a) it can be observed that the spherical pore size of PMMA is around 15.1 μm. The pore size of PVC is around 7.08 μm which is approximately half that of PMMA. As expected, the pore size increases for PMMA–PVC polymer blends and the average diameter of these particles is 27.9 μm. The tendency of PMMA and PVC to join is revealed by the change in shape of particles from spherical to rectangular shape. As a result, PMMA is coordinated with PVC and forms complexation. It can be observed by comparing Fig. 4(c)–(f) that the pore size of PMMA–PVC much smaller than PMMA–PVC with adulteration of LiTFSI. This suggests the presence of structural reorganizations of polymer chain and leads to Li^+ ion transportation in the polymer matrix.

The effect of variation in ratio of PMMA and PVC is also studied. It can be seen from Fig. 4(d)–(f) that PE 3 has a better pore surface distribution than PE 5 and PE 9. It can be inferred that the polymer matrix is in homogenous condition and agglomeration of similar phase of PVC is lesser at high PMMA content. Therefore, phase separation is absent in this polymer electrolyte system. As a result, the charge carriers can be transported quickly and easily without the presence of blocking phase and hence the highest ionic conductivity is observed for PE 3. The highest ionic conductivity is also ascribed to the highest porosity. As observed in Fig. 4(d), the porosity of PE 3 is larger than PE 5 and PE 9. It can therefore be proved that these voids promote the migration of ions and enhance the ionic conductivity of polymer electrolytes [8].

As shown in Fig. 4(e) spherules with average particles size of 0.4 μm are aggregated. As discussed earlier, the formation of globular agglomeration of similar phase of PVC at high PVC loadings ultimately leads to the formation of phase separation. Eventually, this phase separation hinders the migration of Li^+ in the polymer matrix which in turn reduces the ionic conductivity. Stephan et al. suggests that the higher pore size leads to lesser phase segregation and forms a more homogeneous polymer electrolytes system [28]. Similar trend is observed for PE 5 and PE 9. The average pore size of PE 5 and PE 9 is 14.5 and 10.6 μm, respectively. As PMMA loadings decrease, it tends to increase the driving force for phase separation at 90 wt% PVC content. Therefore, ion transportation is

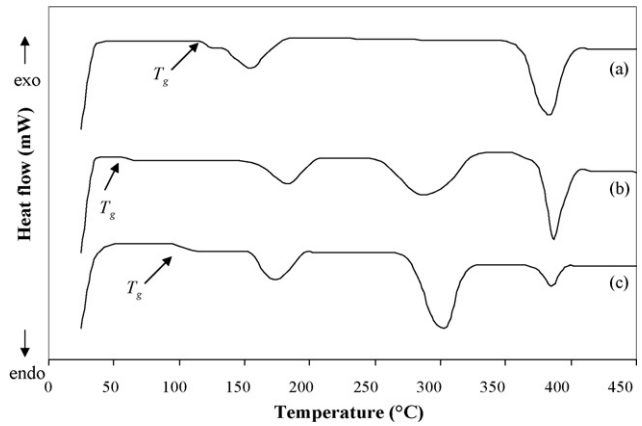

Fig. 5. DSC thermograms of (a) pure PMMA, (b) pure PVC and (c) PMMA–PVC.

less favored in this system and hence the porosity is relatively lesser than PE 5. As a result, lowest ionic conductivity is achieved by PE 9 as discussed in Section 3.1.

3.4. Differential scanning calorimetry (DSC) studies

The DSC measurements are tabulated in Table 1. The DSC thermograms of pure PMMA, pure PVC, PMMA–PVC and PMMA–PVC blend-based polymer electrolytes are shown in Figs. 5 and 6. The following trend is observed in all the DSC thermograms. An endothermic reaction T_g is observed which is then followed by T_m and T_d upon heating the samples further. Apparently, only one T_g is displayed for PMMA–PVC polymer blend and this indicates the homogeneous behavior of the polymer electrolyte [29]. In addition, T_g decreases upon incorporation of PVC due to the interaction between PMMA and PVC via cross-linking. In contrast, T_m has been found to fall in the range of T_m values of PMMA and PVC as well as T_d values. One distinct endothermic peak T_m is illustrated in Fig. 5. This broad peak is due to the overlapping of the melting points of PMMA and PVC. Two endothermic peaks are observed thereafter. These peaks are known as decomposition temperature T_d. The first intense peak is related to the dehydrochlorination of PVC [21], whereas the degradation of unsaturated group of PMMA and the degradation of PVC contribute to second endothermic decomposition peak [29]. According to Fig. 6, T_g is increased with the addition of LiTFSI. The shift towards higher temperature is due to the Li^+ preferring to interact with electron-rich coordinating groups, such as –O– and carbonyl group via transient cross-linkage bonds. These cross-linkage bonds obstruct the rotation of polymer segments and

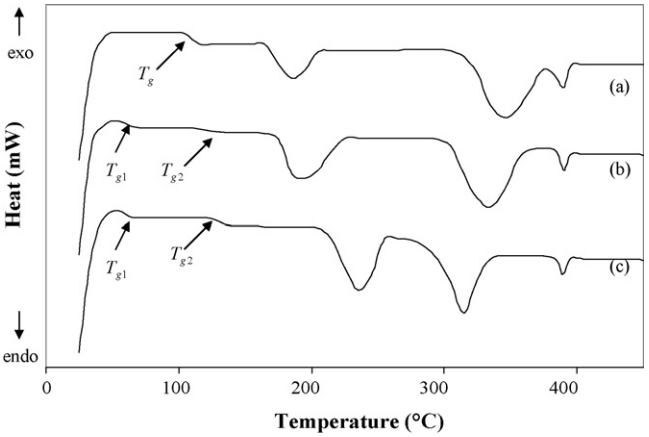

Fig. 6. DSC thermograms of (a) PE 3, (b) PE 5 and (c) PE 9.

hence increase the energy barrier to the segmental movement. Eventually, this Li^+–O^- binding reduces the flexibility of polymer backbone [23,25].

Moreover, the effect of higher loading of PVC onto DSC analyses is also investigated in order to determine the most compatible ratio of PMMA and PVC polymer blends. As shown in Fig. 6, a single value for T_g is obtained for PE 3 whereas two values for T_g are obtained for PE 5 and PE 9. T_{g1} and T_{g2} correspond to the T_g values of PVC and PMMA, respectively. It shows the presence of phase separation of PMMA and PVC. This result is in agreement with the SEM results. This phase separation is mainly due to the slow evaporation of polymer solutions during preparation. The slow increase of polymer concentration up to the solid state induces inhomogeneities in the polymer matrix. This is due to the polymer matrix having sufficient time to separate which in turn promotes the phase segregation [30]. At high PVC loadings, the agglomeration of similar phase of PVC happens and thus leads to the formation of inhibitors into the polymer segments. Such blocking region reduces the flexibility of polymer chain and contributes to the lower segmental motion of polymeric chain. Eventually, lower ionic conductivity is obtained for PE 5 and PE 9. Apart from that, there is an increase in viscosity with increasing PVC concentration. High viscosity of polymer matrix leads to increase in rotation barriers between the polymer segments and thus the flexibility is affected. Therefore, the ion diffusivity is reduced and contributes to lower ionic conductivity [31].

Excessive PVC adulteration enhances the dehydrochlorination process, thus promoting the cross-linking between polymer segments. This leads to insufficient flexibility of polymer chain and impedes the ion transportation [21]. The detailed mechanism for cross-linking of PMMA and PVC is shown in Fig. 7. Degrading products such as Cl free radical and HCl are produced initially upon combustion. For further propagation, these free radicals are favored to react with the methoxyl group of PMMA due to the resonance effect leading to dehydrochlorination process. At the same time, these radicals abstract hydrogen from PVC and produces HCl. These macroradical products from dehydrochlorination process react with each other and eventually form a cross-linkage between PMMA and PVC as shown in the termination process.

PE 3 shows the lowest T_g compared to PE 5 and PE 9. T_g is defined as the transition of temperature from glassy state to rubbery state. Beyond this transition, a long range molecular motion occurs and thus the degree of rotational freedom increases. As a result, the decrease in T_g helps in the softening of the polymer backbone and improves the segmental movement of polymer chains [25,32]. Hence the ions flow more easily throughout the polymer chain. This enhances the ion transportation which achieves the highest ionic conductivity for PE 3. A discrete trend is also illustrated in Fig. 6. In principle, polymer with higher crystalline region should have a higher melting point and heat of fusion [33]. As shown in Fig. 6, T_m increases significantly with increase in the PVC content. Obviously, the heat of fusion also increases upon addition of PVC loadings. PE 3 exhibits lowest T_m and heat of fusion, thus indicating the lowest crystallinity of PE 3 as proven in XRD and SEM studies.

However, T_d is decreased upon further addition of PVC. PE 3 exhibits highest T_m and T_d as tabulated in Table 1. These results suggest that PE 3 has excellent thermal properties than PE 5 and PE 9. It can be concluded from this study that 70 wt% of PMMA blended with 30 wt% PVC is the most compatible ratio.

3.5. Thermogravimetric analysis (TGA) studies

Figs. 8 and 9 depict thermogravimetric analyses of pure PMMA, pure PVC, PMMA–PVC and PMMA–PVC blend-based polymer elec-

Initiation:

Step 1: Degrading product from PVC after combustion, that is Cl free radical

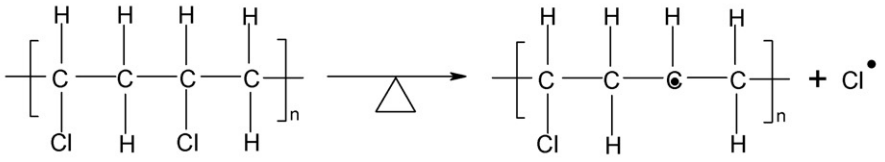

Propagation:

Step 2: Dehyrochlorination is happened where the free radical reacts with PMMA. This free radicals attack the carbon at methoxyl group due to the resonance effect.

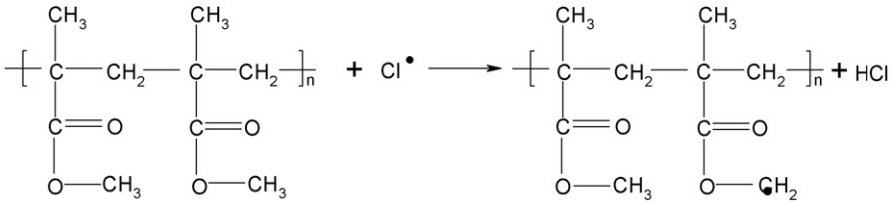

Step 3: The free radical abstracts hyrogen from PVC.

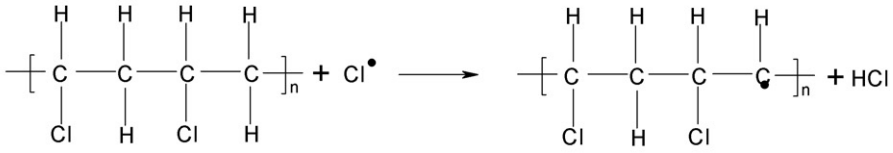

Termination:

Step 4: The product from step 3 is cross-linked with products of PMMA from step 2 PMMA

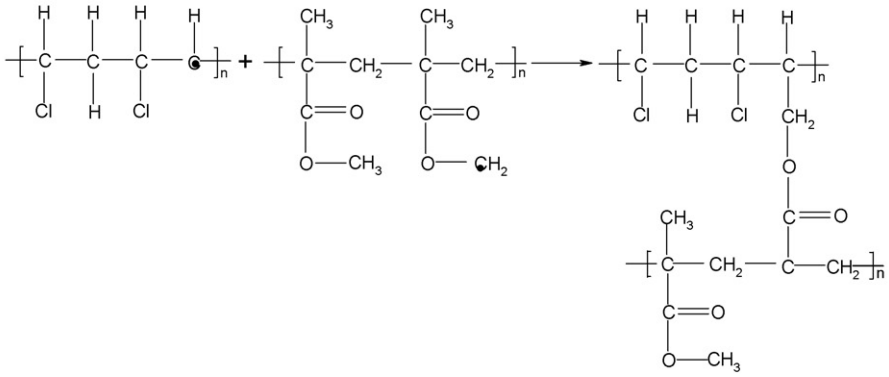

Fig. 7. Mechanisms of cross-linking of PMMA and PVC.

trolytes. The occurrence of stable weight for temperatures of up to 100 °C for all the weights of thin films indicates that the sample has almost dried [25]. Based on the TGA curves, all the thin films have shown 3 stages, except for pure PMMA compound. The initial weight loss of 4% at 167 °C for pure PMMA and weight loss of 2% at 148 °C for pure PVC sample is illustrated in Fig. 8. However, PMMA–PVC blend has a weight loss of 2% at 152 °C. The evaporation of residual solvent, moisture and impurities are mainly due to fluorine. Fluorine is also the contributor for the initial weight loss, as the polymer tends to absorb moisture from its surroundings [25]. A dramatic drop in weight is observed for the second weight loss. The pure PMMA thin film looses 82% weight at 387 °C with a residual mass of 11%. This weight loss is attributed to the degradation of unsaturated group of PMMA as proven in DSC thermograms.

On the contrary, after complete dehydration, the second and final weight loss of PVC is 52% at 256 °C and 6% at 336 °C, respectively. The residual mass of PVC is about 39% decomposition at 386 °C. The second and final weight loss of PVC might be due to the volatilization of monomers, oligomers and dehydrochlorination. For PMMA–PVC blends, the baseline remains stable until 252 °C and this is followed by second and final weight losses. The second and final weight loss of 58% at 342 °C and 13% at 396 °C with a residue mass of 28% was observed. It is observed that blending of PMMA with PVC enhances the thermal stability of polymers at higher decomposition temperature. The second significant weight loss may be due to the unzipping process which contributes to a reduction in molecular weight of polymer chain at high temperature. This unzipping reaction induces many degradation reactions such as random chain scission reaction, depolymerization, inter-

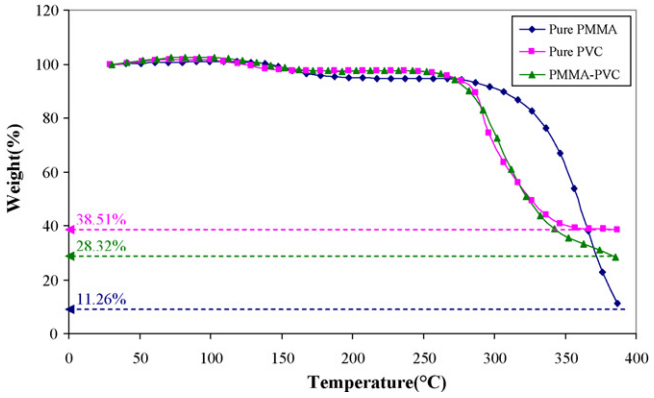

Fig. 8. Thermogravimetric analysis of pure PMMA, pure PVC and PMMA–PVC.

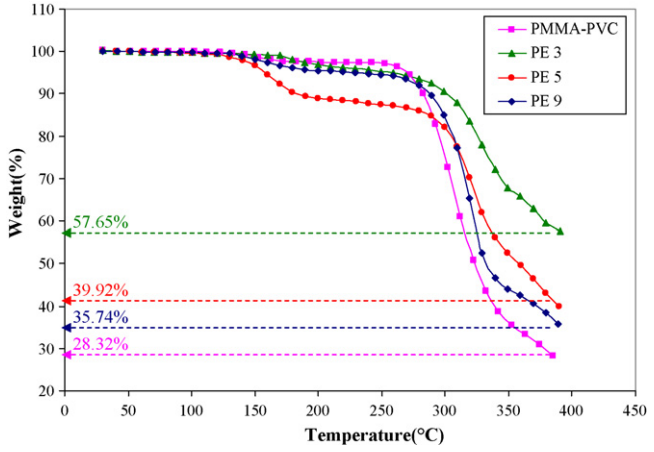

Fig. 9. Thermogravimetric analysis of PMMA–PVC, PE 3, PE 5 and PE 9.

molecular transfer reaction and intra-molecular transfer reaction whereby dimers, trimers and oligomers are produced as well as polymer fragments [21]. As a result, the monomer and oligomers which chemi-adsorbed onto the polymer matrix is volatilized in this region. Dehydrochlorination of PVC might also be attributing to this mass loss. The final weight loss corresponds to the degradation of unsaturated PMMA and PVC for PMMA–PVC polymer blends.

As shown in Fig. 9, the first weight loss of around 11 and 4% are obtained for PE 5 and PE 9, respectively. Beyond the first weight loss, the sample has a drastic weight loss of 56 and 49% for PE 5 and PE 9 respectively at about 269 °C. They are followed by a gradual fall in weight starting at 339 °C. At 389 °C, PE 5 has lost around 16% of its weight with around 40% residual mass, whereas for PE 9 it is around 11% with 36% residual mass. However, the weight loss of the sample is remarkably low for PE 3. Based on the TGA curve, the initial weight loss of PE 3 is around 3% followed by a modest weight loss of 29% which starts at 279 °C until 349 °C. At 390 °C, the residual weight of PE 3 is still around 58% with a loss of 10%. As discussed earlier, the first weight loss is due to the evaporation of retained solvent, moisture and impurities which is mainly due to the fluorine compound from LiTFSI salt. The second weight loss is ascribed to dehyrochlorination of PVC which leads to the volatilization of monomers and oligomers. The degradation of PVC and the elimination of the degrading unsaturated functional group of PMMA are the contributors for final weight loss. In conclusion, with the increase in the decomposition temperature PE 3 shows a better thermal stability than PE 5 and PE 9 with a smaller weight loss.

4. Conclusion

In this study, PMMA–PVC blend-based polymer electrolytes are prepared by solution casting technique. The results obtained in these studies show that a 70 wt% of PMMA blended with 30 wt% of PVC, denoted as PE 3, is a promising candidate for PMMA–PVC blend-based polymer electrolytes. These thin films exhibit Arrhenius behavior where the hopping mechanism is favored. The studies done using XRD and SEM reveal the inherent amorphous properties of PE 3. Phase segregation is absent in PE 3 polymer matrix and this had been proven in SEM and DSC analyses. DSC analyses show that T_g and T_m of PE 3 are lowered whereas T_d is enhanced. This indicates the improvement of thermal properties of polymer electrolytes. By analyzing the TGA thermograms, it can be seen that PE 3 exhibits good thermal stability compared to PE 5 and PE 9.

Acknowledgement

This work was supported by the Malaysia Toray Science Foundation (MTSF).

References

[1] F.M. Gray, Solid Polymer Electrolytes: Fundamentals of Technological Applications, Wiley-VCH, United Kingdom, 1991, pp. 1–30.
[2] S. Ahmad, S. Ahmad, S.A. Agnihotry, J. Power Sources 140 (2005) 151–156.
[3] S. Ramesh, T.F. Yuen, C.J. Shen, Spectrochim. Acta Part A 69 (2008) 670–675.
[4] S. Ramesh, M.F. Chai, Mater. Sci. Eng. B 139 (2007) 240–245.
[5] S. Ramesh, T. Winie, A.K. Arof, Eur. Polym. J. 43 (2007) 1963–1968.
[6] J. Adebahr, N. Byrne, M. Forsyth, D.R. MacFarlane, P. Jacobsson, Electrochim. Acta 48 (2003) 2099–2103.
[7] I. Nicotera, L. Coppola, C. Oliviero, M. Castriota, E. Cazzanelli, Solid State Ionics 177 (2006) 581–588.
[8] R. Baskaran, S. Selvasekarapandian, N. Kuwata, J. Kawamura, T. Hattori, J. Phys. Chem. Solids 68 (2007) 407–412.
[9] S. Rajendran, M. Sivakumar, R. Subadevi, Mater. Lett. 58 (2004) 641–649.
[10] V. Aravindan, C. Lakshmi, P. Vickraman, Curr. Appl. Phys. 9 (2009) 1106–1111.
[11] H.S. Han, H.R. Kang, S.W. Kim, H.T. Kim, J. Power Sources 112 (2002) 461–468.
[12] D.W. Xia, D. Soltz, J. Smid, Solid State Ionics 14 (1984) 221.
[13] N. Kobayashi, M. Uchiyama, K. Shigehara, E. Tsuchida, J. Phys. Chem. 89 (1985) 987.
[14] M. Watanable, S. Nagano, K. Sanvi, N. Ogata, J. Power Sources 20 (1987) 327.
[15] J.R. MacCallum, M.J. Smith, C.A. Vincent, Solid State Ionics 11 (1987) 307.
[16] T. Uma, T. Mahalingam, U. Stimming, Mater. Chem. Phys. 90 (2005) 245–249.
[17] P. Meneghetti, S. Qutubuddin, A. Webber, Electrochim. Acta 49 (2004) 4923–4931.
[18] R. Kumara, A. Subramania, N.T.K. Sundaram, G.V. Kumar, I. Baskaran, J. Membr. Sci. 300 (2007) 104–110.
[19] K.S. Kum, M.K. Song, Y.T. Kim, H.S. Kim, B.W. Cho, H.W. Rhee, Electrochim. Acta 50 (2004) 285–288.
[20] S. Rajendran, O. Mahendran, R. Kannan, Fuel 81 (2002) 1077–1081.
[21] Z. Ahmad, N.A. Al-Awadi, F. Al-Sagheer, Polym. Degrad. Stabil. 92 (2007) 1025–1033.
[22] S. Rajendran, T. Uma, J. Power Sources 88 (2002) 282–285.
[23] W. Li, M. Yuan, M. Yang, Eur. Polym. J. 42 (2006) 1396–1402.
[24] V.B. Achari, T.J.R. Reddy, A.K. Sharma, V.V.R.N. Rao, Ionics 13 (2007) 349–354.
[25] S. Ramesh, A.K. Arof, J. Power Sources 99 (2001) 41–47.
[26] R. Baskaran, S. Selvasekarapandian, N. Kuwata, J. Kawamura, T. Hattori, Solid State Ionics 177 (2006) 2679–2682.
[27] S. Ganesan, B. Muthuraaman, V. Mathew, J. Madhavan, P. Maruthamuthu, S. Austin Sunthanthiraraj, Sol. Energy Mater. Sol. Cells 92 (2008) 1718–1722.
[28] A.M. Stephan, T.P. Kumar, N.G. Renganathan, S. Pitchumani, R. Thirunakaran, N. Muniyandi, J. Power Sources 89 (2000) 80–87.
[29] S. Ahmad, H.B. Bohidar, S. Ahmad, S.A. Agnihotry, Polymer 47 (2006) 3583–3590.
[30] D. Braun, H. Cherdron, M. Rehahn, H. Ritter, B. Voit, Polymer Synthesis: Theory and Practice, Springer, Berlin, 2005, pp. 124–126.
[31] Y. Yang, C.H. Zhou, S. Xu, H. Hu, B. Lei Chen, J. Zhang, S.J. Wu, W. Liu, X.Z. Zhao, J. Power Sources 185 (2008) 1492–1498.
[32] A.M. Stephan, Y. Saito, N. Muniyandi, N.G. Renganathan, S. Kalyanasundaram, R.N. Elizabeth, Solid State Ionics 148 (2002) 467–473.
[33] J.M. Yang, H.Z. Wang, C.C. Yang, J. Membr. Sci. 322 (2008) 74–80.